Nanoengineering Opens a New Era for Tungsten as Well

Q. Wei, K.T. Ramesh, B.E. Schuster, L.J. Kecskes, and R.J. Dowding

For the past century, tungsten has been exploited for numerous applications due to its unique properties, including its extremely high melting point, mass density, and mechanical strength. One specific potential application of tungsten (owing to its high mass density and strength) is the replacement of depleted uranium within kinetic energy anti-armor penetrators. Strenuous efforts in this direction have had limited success. However, nanoengineering has been applied recently to tailor the microstructure and properties of tungsten, leading to dramatic improvement with regard to this application. This paper provides some recent results on nanoengineered tungsten and discusses the underlying principles. It appears that nanoengineering is opening a new era for tungsten.

INTRODUCTION

Nanoengineering is the practice of engineering at the nanometer scale (a nanometer is one-billionth of a meter, or 1 nm = 10^{-9} m). The history of nanoengineering can be traced back to the end of the 1950s when the Nobel Prize Laureate Richard Feynman gave his famous speech "There is plenty of room at the bottom."[1] About one decade prior to Feynman's speech, metallurgists had already recognized the strong effect of reducing grain size on the behavior of metals and alloys.[2,3] It is now almost common sense that metals with grain size in the ultrafine-grained (UFG, grain size d smaller than 500 nm but greater than 100 nm) and nanocrystalline (NC, d<100 nm) regimes have much greater strength than their coarse-grained (CG) counterparts. Accompanying the high strength is a loss of tensile ductility,[4–6] which has recently been considered to be induced by artificial defects.[7–11] The focus of investigations has recently shifted to other unusual properties of UFG/NC metals, including the retained ductility via some special processing routes.[7–9,11,12]

There are a number of ways to make UFG/NC metals. The bottom-up methods involve producing nanosize particles followed by consolidation, while the top-down methods start with a bulk CG metal and refine the grain size into the

Figure 1. (a) An optical micrograph of ECAP tungsten (four passes at 1,000°C) showing refined microstructure due to severe plastic deformation. Notice that the pre-existing grain boundaries are still visible. (b) After further rolling at relatively low temperatures, the microstructure is refined into the UFG regime. Selected area diffraction pattern (not shown here) indicates that many grain boundaries are of the low-angle type.

UFG/NC regimes. The most direct cause of the loss of ductility is the introduction of volume defects such as residual porosity, poor inter-particle bonding due to impurity contamination, etc.[13] Many of these effects are a consequence of so-called "two-step" processing (usually bottom-up) where UFG/NC powders are produced followed by hot compaction. One strategy to mitigate such detrimental effects is "one-step" processing where handling of powders in open air is avoided, or the starting material is in fully dense, bulk forms (top-down). Koch and co-workers have demonstrated that NC copper with d~20 nm produced by in-situ consolidation can have tensile elongation >10%.[8] Another technique for the production of UFG/NC metals is severe plastic deformation (SPD), where a fully dense work piece is subjected to very large amounts of plastic strain.[14] This avoids the handling of powders and subsequent consolidation, and is therefore a one-step, top-down process. Very recently, a bi-modal grain size distribution has manifested both significant strength and tensile elongation, where the NC grains serve as the strengthening medium and the large (d a few micrometers) grains accommodate the plasticity.[10,11] This concept has since been used in other systems.[15]

The majority of nanoengineering efforts are on metals of face-centered-cubic (fcc) structures such as aluminum, copper, and nickel.[16] Much less work has been conducted on body-centered-cubic (bcc) metals. One reason is the difficulty in refining the grain size of bcc metals into the UFG/NC regimes. Recent efforts have shown that UFG/NC bcc metals exhibit some very unique behavior compared to their fcc counterparts.[17–27] For example, UFG/NC iron exhibits localized shearing even under quasi-static

$$\frac{\chi_{SB}}{a/m} = \min\left\{1, \frac{1}{(n/m) + \sqrt{n/m}}\right\} \quad (1)$$

$$\chi_{SB} = \frac{a}{m} = \frac{\lambda\sigma_0}{\rho cm} \quad (2)$$

compression.[17,28,29] Nanocrystalline vanadium fails in a manner similar to metallic glasses under dynamic compression.[20] Such deformation and failure modes are desirable for a kinetic energy (KE) penetrator material. There has been tremendous research work in search of a replacement for depleted uranium (DU) for the making of such penetrators, and among all the candidates, tungsten, a bcc metal, seems to be the best in terms of its mass density rivaling DU.[30]

Body-centered-cubic metals are known to be very vulnerable to soluble interstitial impurities which have been held responsible for their brittle failure at low homologous temperatures (the homologous temperature is the temperature of interest divided by the melting point of the specific metal).[31] Tungsten is the most notorious in this respect. Conventional powder metallurgy (P/M) CG tungsten exhibits a very high ductile-to-brittle transition temperature (DBTT) of around 150°C.[32] Efforts to produce UFG/NC tungsten through P/M have had little success to this point. Very recently, the authors have shown that SPD-based nanoengineering may be an alternative for tungsten.[23,24,33] This article reports and reviews the application of nano-engineering to commercial-purity tungsten, demonstrating strong evidence of adiabatic shear banding (ASB), which is the basis for the desired performance of a KE penetrator. A progressive methodology was adopted in which tungsten with a UFG microstructure was processed and examined, and then nano-engineered tungsten was investigated.

See the sidebar for details on strategy and methodology.

EXPERIMENTAL DEMONSTRATIONS OF PRINCIPLE

Figure 1a shows the microstructure of tungsten after four passes of equal-channel angular pressing (ECAP). Since the starting material has a grain size of ~40 μm, grain size reduction by ECAP is obvious. However, ECAP at 1,000°C can only refine the grain size of tungsten down to a few micrometers due to dynamic recrystallization and grain growth. To further refine the grain size, the ECAP tungsten was rolled at 800°C and below. Figure 1b displays the transmission-electron microscopy (TEM) micrograph of tungsten that was further rolled at 600°C to introduce an additional strain of 1.8. The average grain size (or sub-grain size) is around 500 nm, thus in the UFG regime.

Figure 2a displays a typical microstructure of high-pressure torsion (HPT) processed tungsten. The average grain size derived from TEM micrographs is about 100 nm. The selected area diffraction pattern (Figure 2b) shows almost continuous rings, indicating the absence of preferential orientation of the grains (texturing). Figure 2c is a typical high-resolution TEM (HRTEM) image of a grain boundary (GB). A few interesting characteristics can be identified with this GB. First, it is of large-angle type. Second, it has a number of atomic facets, steps or ledges, suggesting its high energy and non-equilibrium nature.[37–39] Third, no GB phase, amorphous or crystalline, can be associated with the GB. In other words, the crystalline structure of the constituent grains is disrupted only by the presence of the GB, and the GB is clean and well defined. An HRTEM of the same specimen also reveals the existence of a large number of edge dislocations in the vicinity of the GB (not shown here).[33] This is unusual since the plasticity of tungsten at such low temperature is usually accommodated by screw dislocations by means of the double-kink mechanism, and only straight screws were observed by TEM after finite plastic deformation.[40]

Figure 3a shows the quasi-static and dynamic stress-strain curves of tungsten specimens processed by ECAP and ECAP+rolling (referred to henceforth as ECAP+R tungsten). The following observations can be derived. First, ECAP
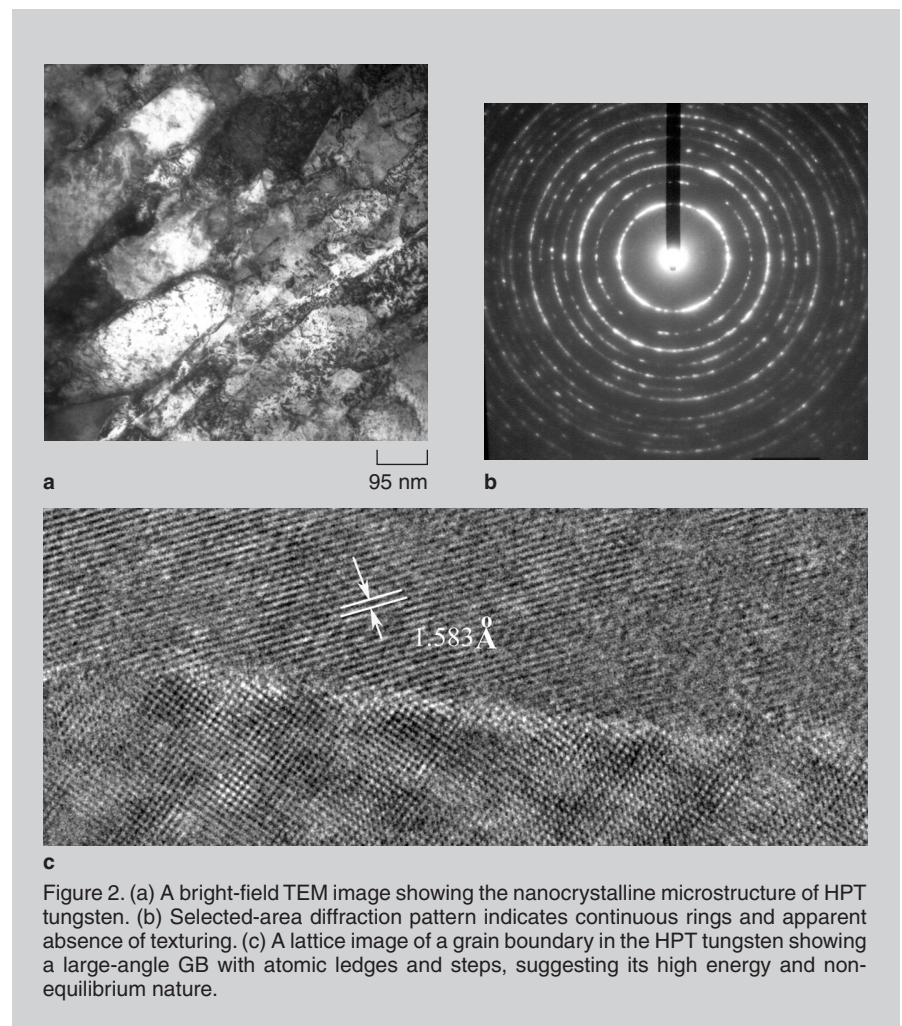

Figure 2. (a) A bright-field TEM image showing the nanocrystalline microstructure of HPT tungsten. (b) Selected-area diffraction pattern indicates continuous rings and apparent absence of texturing. (c) A lattice image of a grain boundary in the HPT tungsten showing a large-angle GB with atomic ledges and steps, suggesting its high energy and non-equilibrium nature.

STRATEGY AND METHODOLOGY

Severe plastic deformation (SPD)[14] is used to progressively refine the grain size of commercial-purity tungsten. First, equal-channel-angular-pressing (ECAP) is used followed by low-temperature rolling for the production of ultra-fine grain tungsten. Details of ECAP can be found in, for example, Reference 14. In this technique, the work piece is pushed through two connecting channels with the same cross-sectional area. With a right connecting angle the work piece experiences an equivalent strain of ~1.0 with each pass of ECAP. The recrystallization temperature of tungsten is around 1,250°C for moderate plastic deformation.[31] To ensure the efficiency of grain size reduction, ECAP was performed at 1,000°C. To alleviate oxidation of the tungsten work piece, the tungsten rod was encapsulated in a stainless-steel canister. The die angle (or connecting angle between the channels) is 120° to avoid cracking of tungsten. Another SPD technique used is high-pressure torsion (HPT),[14,34] where a disk of tungsten (~10 mm in diameter and ~1.0 mm in thickness) is subjected to high pressure (~4 GPa) while torsion is applied to it, allowing a tremendous amount of plastic strain to be pumped into the material (a full turn gives an equivalent strain of ~18 at the edge of the disk with the above dimension). In this work, HPT was performed at 500°C, much lower than the recrystallization temperature of tungsten. Details can be found in Reference 33.

Scanning-electron microscopy and optical microscopy are used to examine the post-loading specimen surface to identify the deformation and failure mechanisms. Transmission-electron microscopy is used to analyze grain size, defects, and their distributions, and the grain boundary structure.

The processed tungsten was tested under uni-axial quasi-static (strain rate 10^{-4} s^{-1} to 10^0 s^{-1}) and dynamic compression (using split-Hopkinson pressure bar (SHPB), strain rate ~10^3 s^{-1}).[35] For the HPT-processed tungsten, due to the limited dimension of the disk, a miniaturized SHPB system (or desk-top Kolsky bar)[36] was used to obtain the dynamic data.

at 1,000°C (six passes) has increased the quasi-static strength to 1.5 times that of the control CG tungsten sample (apparent compressive yield strength of CG tungsten is ~1.0 GPa). Further low-temperature rolling has increased the strength to nearly twice its CG value. Second, work hardening of the SPD-processed tungsten is considerably reduced. Furthermore, under dynamic compression, SPD tungsten shows flow softening at quite small plastic strains, in sharp contrast to the CG tungsten where under dynamic loading slight apparent hardening is observed. This flow softening, especially in the ECAP+R tungsten, is due to a change in deformation mode, as detailed later in this paper.

Microhardness measurement on the HPT tungsten shows that the nano-tungsten is super strong with a hardness value around 11 GPa at the rim of the disk.[33] This hardness value is remarkable even when compared with some strong ceramics (e.g., the hardness of sintered Si_3N_4 ceramic is about 20 GPa).[41] Quasi-static compression of the HPT tungsten showed a yield strength ~3.5 GPa, in accordance with the hardness value if the Tabor relation[42] between Vicker's hardness (VHN) and yield strength of an isotropic material is assumed (VHN≈3σ_y). Figure 3b displays a few dynamic stress-strain

curves of HPT tungsten (data recorded using the miniature split-Hopkinson pressure bar SHPB technique). The most salient feature in these curves is the very early precipitous stress collapse, which is one of the most desirable properties for a penetrator material.

Under quasi-static and dynamic compression, conventional CG tungsten and extruded tungsten (extrusion at 1,200°C) that shows strength levels close to the ECAP tungsten presented here exhibits axial cracks (cracks parallel to the loading axis).[43] The ECAP tungsten in this study exhibits similar behavior.[24] Most of the cracks are along the pre-existing grain boundaries, consistent with tensile behavior of such tungsten where failure occurs at a stress level about only half that of compression and with no evidence of plastic deformation, similar to that of most ceramics.

Figure 4a is a post-dynamic loading optical micrograph of an ECAP+R tungsten, with the corresponding stress-strain response shown in Figure 3a. Instead of axial cracks, clear evidence of shear bands is observed. Higher-magnification SEM imaging (Figure 4b, for example) indicates severe and localized adiabatic shear flow within the ASBs. Polishing of the roughened surface followed by chemical etching reveals the detailed microstructure of the shear bands, includ-

ing density and direction of the shear lines, width of the shear bands (around 40 µm), and cracking along the central line of the shear bands (Figure 4b). High-speed photography (not shown here) indicates that the stress-collapse in the stress-strain curves roughly corresponds to the initiation of ASBs.[24] The strain level at which ASB kicks in is around 0.1 (10%). The ASBs are fully developed at a strain level of ~15%. The onset of secondary shear bands was also observed via high-speed photography.[24]

Figure 5a displays a post-dynamic loading optical micrograph of the HPT nano-tungsten. Again, instead of axial cracking, a localized shear band is observed, subtending an angle of ~45° to the loading direction (horizontal in this case). The SEM micrograph of Figure 5b shows the severe curving of the pre-existing scratches introduced during specimen preparation prior to dynamic loading. In this case, the shear band width (about 5 µm) is much smaller compared to that of the UFG tungsten (ECAP+RW). In other UFG/NC bcc metals such as iron, a change of shear band width with grain size is also observed; the underlying mechanism is still under investigation. Figure 5b also shows a crack as a consequence of highly localized adiabatic shearing.

As pointed out earlier in this paper, because of their high mass density, tungsten and tungsten heavy alloys have been investigated extensively for the production of anti-armor KE penetrators in place of DU. However, most of the efforts have had limited success, mainly due to the lack of plasticity and poor propensity for ASB in conventional CG tungsten. On one hand, plastic deformation is needed to introduce adiabatic heating, a prerequisite for the development of ASB. On the other hand, uniform plastic deformation of the penetrator material is to be avoided so that the kinetic energy can be used primarily for penetration. Uniform plastic deformation of the penetrator material is responsible for "mushrooming" of the penetrator head, in contrast to "self-sharpening" where the head remains sharp and failed penetrator material is discarded away via adiabatic shearing, thus leaving a small penetration channel within the target. The self-sharpening effect of the penetrator is rooted in the material property of shear

band susceptibility in that under dynamic loading, the plastic deformation is highly concentrated in a narrow region.[30]

Soluble interstitial impurities such as carbon, nitrogen, and sulfur[31] segregate along the GBs to render the GBs the weak links under mechanical straining, leading to grain boundary embrittlement. However, brittle behavior is not intrinsic to tungsten, since experimental results have shown that single-crystal tungsten can be deformed to significant plastic strain under tension even at 77K.[44] Therefore, if the pre-existing detrimental impurities at the GBs can somehow be depleted, ductility may be improved. One strategy to furnish this is by means of grain boundary engineering.[45] If more GBs are created in addition to the pre-existing GBs, and if appropriate kinetic condition is provided for the pre-existing GB impurities to diffuse away and be relocated to the newly created GBs, the average impurity concentration at the GBs can be reduced. This will increase the GB strength and reinstate the ductility. The most efficient way to induce more GBs without worsening impurity contamination is a top-down route such
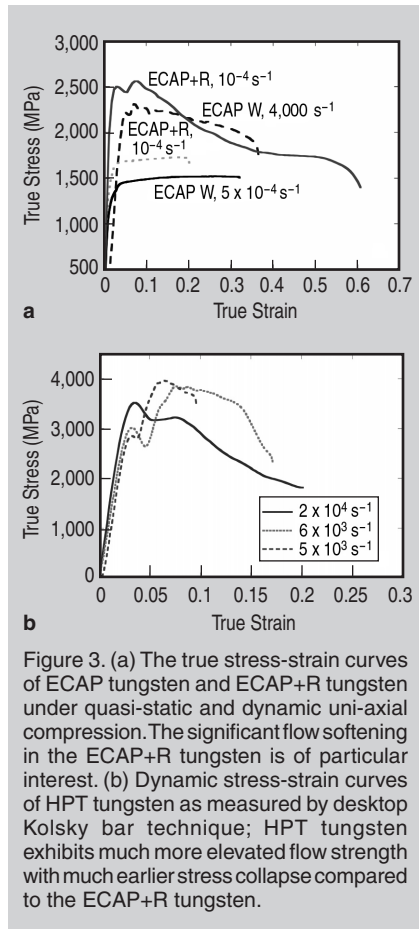
Figure 3. (a) The true stress-strain curves of ECAP tungsten and ECAP+R tungsten under quasi-static and dynamic uni-axial compression. The significant flow softening in the ECAP+R tungsten is of particular interest. (b) Dynamic stress-strain curves of HPT tungsten as measured by desktop Kolsky bar technique; HPT tungsten exhibits much more elevated flow strength with much earlier stress collapse compared to the ECAP+R tungsten.

as SPD. It has been borne out that the GBs induced by SPD have some special properties.[39] For instance, they are of non-equilibrium and high-energy nature. Such GBs are ideal hosting sites for interstitial impurities. It has also been proposed that the peculiar nature of the SPD-induced GBs explains the paradox of many UFG/NC metals where significant ductility is observed concurrently with high strength.[46]

Another contributing factor to the reinstated ductility of the SPD nanoengineered tungsten might be the numerous edge dislocations observed in HRTEM in the proximity of the GBs.[33] Systematic work by Gumbsch et al.[47] on the controlling factors for the fracture toughness and brittle-to-ductile transition in single-crystal tungsten indicates that pre-plastic-deformation of the specimen can increase both low- and high-temperature fracture toughness. Particularly, much improved high-temperature fracture toughness has been achieved by pre-plastic-deformation. They pointed out that if a dislocation (either generated at the crack tip or a pre-existing one) moves in the stress field along the crack tip, it will generate dislocation segments of non-screw (and thus highly mobile) character parallel to the crack tip. High-resolution TEM shows a presence of residual edge dislocations in the HPT nano-tungsten.[33] Such edges may work together with other pre-existing dislocations that are highly mobile so as to provide highly efficient shielding of the crack tip, thus resulting in relatively ductile failure.[33]

Finally, the enhanced propensity for ASB in nano-engineered tungsten must be considered. Mechanistic models have been articulated to predict this propensity in visco-plastic materials. Wright[48] derived Equation 1 (see the Equations table on page 41), where χ_{SB} is the susceptibility to ASB, a is the non-dimensional thermal softening parameter defined by $a = (-\partial\sigma / \partial T) / \rho c$ (σ is the flow stress, T the temperature, ρ the density, and c the specific heat of the material), n the strain hardening exponent, and m the strain rate sensitivity (SRS).

For a perfectly plastic material (no strain hardening) such as the SPD nano-engineered tungsten presented here, the susceptibility reduces to Equation 2, where $\lambda = -(1/\hat{\sigma}_0)\partial\sigma/\partial T$ is the thermal softening parameter evaluated
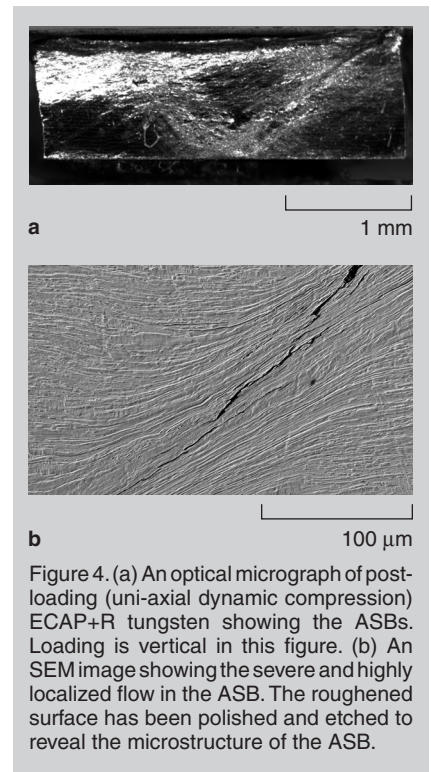
Figure 4. (a) An optical micrograph of post-loading (uni-axial dynamic compression) ECAP+R tungsten showing the ASBs. Loading is vertical in this figure. (b) An SEM image showing the severe and highly localized flow in the ASB. The roughened surface has been polished and etched to reveal the microstructure of the ASB.

under isothermal conditions ($\hat{\sigma}_0$ is a normalizing stress), and σ_0 is the yield strength. Ultra-fine grain/NC metals have much higher yield strength than their CG counterparts (the well-known Hall-Petch effect). Recent experimental results and theoretical analyses have shown that SRS of UFG/NC bcc metals is considerably reduced compared to the CG counterparts.[21] Calculations based on the experimental results and the physical properties of tungsten show that susceptibility to ASB of the UFG/NC tungsten is several orders of magnitude higher than that of conventional CG tungsten.

CONCLUSIONS

This study has applied nanoengineering to produce tungsten with unusual microstructure and mechanical behavior by using a progressive methodology to refine the grain size. Ultrafine-grained tungsten and nanocrystalline tungsten were processed using SPD under various conditions. Mechanical testing under uni-axial dynamic loading showed that such UFG and NC tungsten exhibit the long-sought-after localized shearing, rather than uniform plastic deformation and/or axial cracking. This work shows that nanoengineering is opening a new era for tungsten, particularly for its application in anti-armor kinetic energy penetrators.
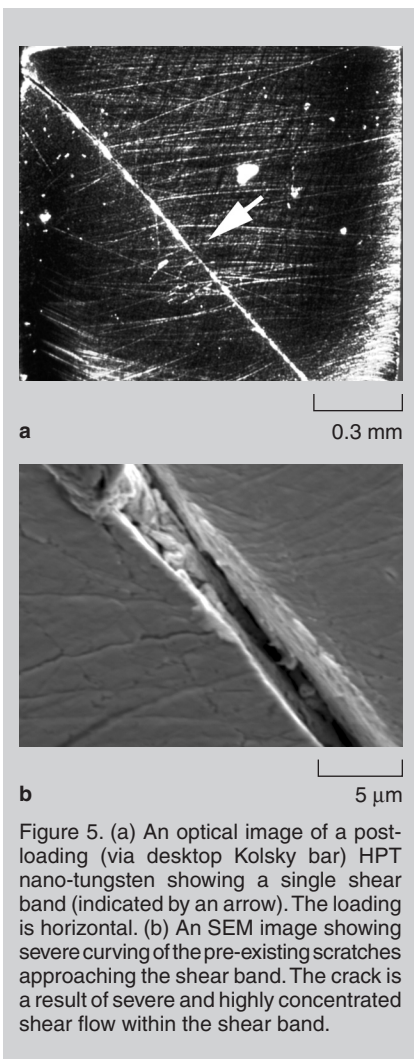
a 0.3 mm

b 5 μm

Figure 5. (a) An optical image of a post-loading (via desktop Kolsky bar) HPT nano-tungsten showing a single shear band (indicated by an arrow). The loading is horizontal. (b) An SEM image showing severe curving of the pre-existing scratches approaching the shear band. The crack is a result of severe and highly concentrated shear flow within the shear band.

References

1. R.P. Feynman, "There is Plenty of Room at the Bottom," *Engineering & Science* (Pasadena, CA: Caltech Public Relations, 1959), cited 2006; *www.zyvex.com/nanotech/feynman.html*.
2. E.O. Hall, "The Deformation and Ageing of Mild Steel: III. Discussion of Results," *P. Phys. Soc. B,* 64 (1951), pp. 747–753.
3. N.J. Petch, "The Cleavage Strength of Polycrystals," *J. Iron and Steel Institute,* 174 (1953), pp. 25–28.
4. C.C. Koch, "Optimization of Strength and Ductility in Nanocrystalline and Ultrafine Grained Metals," *Scripta Mater.,* 49 (2003), pp. 657–662.
5. E. Ma, "Instabilities and Ductility of Nanocrystal-line and Ultrafine-Grained Metals," *Scripta Mater.,* 49 (2003), pp. 663–668.
6. E. Ma, "Controlling Plastic Instability," *Nature Materials,* 2 (2003), pp. 7–8.
7. K.M. Youssef et al., "Ultratough Nanocrystalline Copper with a Narrow Grain Size Distribution," *Appl. Phys. Lett.,* 85 (6) (2004), pp. 929–931.
8. K.M. Youssef et al., "Ultrahigh Strength and High Ductility of Bulk Nanocrystalline Copper," *Appl. Phys. Lett.,* 87 (9) (2005), p. 091904.
9. S. Cheng et al., "Tensile Properties of In Situ Consolidated Nanocrystalline Cu," *Acta Mater.,* 53 (5) (2005), pp. 1521–1533.
10. Y.M. Wang and E. Ma, "Three Strategies to Achieve Uniform Tensile Deformation in a Nanostructured Metal," *Acta Mater.,* 52 (2004), pp. 1699–1709.
11. Y.M. Wang et al., "High Tensile Ductility in a Nanostructured Metal," *Nature,* 419 (2002), pp. 912–915.
12. E. Ma, "Eight Routes to Improve the Tensile Ductility of Bulk Nanostructured Metals and Alloys," *JOM,* 58 (4) (2006), pp. 49–53.
13. C.C. Koch and J. Narayan, "The Inverse Hall-Petch Effect—Fact or Artifact?" *Structure and Mechanical Properties of Nanophase Materials—Theory and Computer Simulations vs. Experiments* (Warrendale, PA: MRS, 2001), ID# 37343 .
14. R.Z. Valiev, R.K. Islamgaliev, and I.V. Alexandrov, "Bulk Nanostructured Materials from Severe Plastic Deformation," *Prog. Mater. Sci.,* 45 (2000), pp. 103–189.
15. D.B. Witkin and E.J. Lavernia, "Synthesis and Mechanical Behavior of Nanostructured Materials via Cryomilling," *Prog. Mater. Sci.,* 51 (2006), pp. 1–60.
16. K.S. Kumar, H. Van Swygenhoven, and S. Suresh, "Mechanical Behavior of Nanocrystalline Metals and Alloys," *Acta Mater.,* 51 (2003), pp. 5743–5774.
17. Q. Wei et al., "Evolution and Microstructure of Shear Bands in Nanostructured Fe," *Appl. Phys. Lett.,* 81 (7) (2002), pp. 1240–1242.
18. Q. Wei et al., "Microstructure and Mechanical Properties of Tantalum after Equal Channel Angular Extrusion (ECAE)," *Mater. Sci. Eng. A,* 358 (1-2) (2003), pp. 266–272.
19. Q. Wei et al., "Adiabatic Shear Banding in Ultrafine Grained Fe Processed by Severe Plastic Deformation," *Acta Mater.,* 52 (7) (2004), pp. 1859–1869.
20. Q. Wei et al., "Nano-Structured Vanadium: Processing and Mechanical Properties under Quasi-Static and Dynamic Compression," *Scripta Materialia,* 50 (3) (2004), pp. 359–364.
21. Q. Wei et al., "Effect of Nanocrystalline and Ultrafine Grain Sizes on the Strain Rate Sensitivity and Activation Volume: fcc versus bcc Metals," *Mater. Sci. Eng. A,* 381 (1-2) (2004), pp. 71–79.
22. Y.J. Wei and L. Anand, "Grain Boundary Sliding and Separation in Polycrystalline Metals: Application to Nanocrystalline fcc Metals," *J. Mechanics and Physics of Solids,* 52 (2004), pp. 2584–2616.
23. Q. Wei et al., "Plastic Flow Localization in Bulk Tungsten with Ultrafine Microstructure," *Appl. Phys. Lett.,* 86 (10) (2005), p. 101907.
24. Q. Wei et al., "Mechanical Behavior and Dynamic Failure of High-Strength Ultrafine Grained Tungsten under Uniaxial Compression," *Acta Mater.,* 54 (1) (2006), pp. 77–87.
25. T.R. Malow and C.C. Koch, "Mechanical Properties in Tension of Mechanically Attrited Nanocrystalline Iron by the Use of Miniaturized Disk Bend Test," *Acta Mater.,* 46 (18) (1998), pp. 6459–6473.
26. T.R. Malow et al., "Compressive Mechanical Behavior of Nanocrystalline Fe Investigated with an Automated Ball Indentation Technique," *Mater. Sci. Eng. A,* 252 (1998), pp. 36–43.
27. J.E. Carsley et al., "Mechanical Behavior of Bulk Nanostructured Iron Alloy," *Metall. Mater. Trans. A,* 29A (1998), pp. 2261–2271.
28. D. Jia, K.T. Ramesh, and E. Ma, "Failure Mode and Dynamic Behavior of Nanophase Iron under Compression," *Scripta Mater.,* 42 (2000), pp. 73–78.
29. D. Jia, K.T. Ramesh, and E. Ma, "Effects of Nano-crystalline and Ultrafine Grain Sizes on Constitutive Behavior and Shear Bands in Iron," *Acta Mater.,* 51 (2) (2003), pp. 3495–3590.
30. L.S. Magness, "An Overview of the Penetration Performances of Tungsten and Depleted Uranium Alloy Penetrators: Ballistic Performances and Metallographic Examinations," *Ballistics 2000* (Lancaster, PA: DEStech Publications, Inc., 2002), CD-ROM..
31. E. Lassner and W.-D. Schubert, *Tungsten-Properties, Chemistry, Technology of the Element, Alloys and Chemical Compounds* (Dordrecht, the Netherlands: Kluwer-Academic/Plenum Publishers, 1998).
32. B.C. Allen, D.J. Maykuth, and R.I. Jaffee, "The Recrystallization and Ductile-Brittle Transition Behavior of Tungsten," *J. Institute of Metals,* 90 (1961), pp. 120–128.
33. Q. Wei et al., "Microstructure and Mechanical Properties of Super-Strong Nanocrystalline Tungsten Processed by High-Pressure Torsion," *Acta Mater.,* 54 (2006), in press.
34. A.P. Zhilyaev et al., "Experimental Parameters Influencing Grain Refinement and Microstructural Evolution during High-Pressure Torsion," *Acta Mater.,* 51 (2003), pp. 753–765.
35. P.S. Follansbee, "High Strain Rate Compression Testing," *ASM Metals Handbook* (Metals Park, OH: American Society of Metals, 1985), p. 190.
36. D. Jia and K.T. Ramesh, "A Rigorous Assessment of the Benefits of Miniaturization in the Kolsky Bar System," *Experimental Mechanics,* 44 (5) (2004), pp. 445–454.
37. R.Z. Valiev, V.Y. Gertsman, and R. Kaibyshev, "Grain Boundary Structure and Properties under External Influence," *Physica Status Solidi A,* 97 (1986), pp. 11–56.
38. R.Z. Valiev, "Nanomaterial Advantage," *Nature,* 419 (2002), pp. 887–889.
39. A.A. Nazarov, A.E. Romanov, and R.Z. Valiev, "On the Structure, Stress Fields and Energy of Nonequilibrium Grain Boundaries," *Acta Metall. Mater.,* 41 (4) (1993), pp. 1033–1040.
40. J.W. Christian, "Some Surprising Features of the Plastic-Deformation of Body-Centered Cubic Metals and Alloys," *Metall. Trans. A,* 14A (1983), p. 1237.
41. P.J. Blau, R.L. Martin, and E.S. Zanoria, "Effects of Surface Grinding Conditions on the Reciprocating Friction and Wear Behavior of Silicon Nitride," *Wear,* 203 (1997), pp. 648–657.
42. D. Tabor, *The Hardness of Metals* (Oxford, U.K.: Clarendon Press, 1951).
43. A.M. Lennon and K.T. Ramesh, "The Thermoviscoplastic Response of Polycrystalline Tungsten in Compression," *Mater. Sci. Eng. A,* 276 (2000), pp. 9–21.
44. A.S. Argon and S.R. Maloof, "Plastic Deformation of Tungsten Single Crystals at Low Temperature," *Acta Metallurgica,* 14 (1966), pp. 1449–1462.
45. T. Watanabe, "An Approach to Grain Boundary Design for Strong and Ductile Polycrystals," *Res. Mechanica,* 11 (1984), pp. 47–84.
46. R.Z. Valiev et al., "Paradox of Strength and Ductility in Metals Processed by Severe Plastic Deformation," *J. Mater. Res.,* 17 (1) (2002), pp. 5–8.
47. P. Gumbsch et al., "Controlling Factors for the Brittle-to-Ductile Transition in Tungsten Single Crystals," *Science,* 282 (5392) (1998), pp. 1293–1295.
48. T.W. Wright, *The Physics and Mathematics of Adiabatic Shear Bands* (Oxford, U.K.: Cambridge Press, 2002).

Q. Wei is with the Department of Mechanical Engineering at the University of North Carolina-Charlotte. K.T. Ramesh is with the Department of Mechanical Engineering at the Johns Hopkins University in Baltimore, Maryland. B.E. Schuster, L.J. Kecskes, and R.J. Dowding are with the U.S. Army Research Laboratory at Aberdeen Proving Ground, Maryland.

For more information, contact Q. Wei, University of North Carolina-Charlotte, Department of Mechanical Engineering, 362 ERB, 9201 University City Blvd., Charlotte, NC 28223; (704) 687-8213; fax: (704) 687-8345; e-mail: qwei@uncc.edu.